8 Mechanisms for tropical rainfall responses to equatorial heating

More reading:

1. Hamouda, M. and Kucharski, F. (2019) Ekman pumping Mechanism driving Precipitation anomalies in Response to Equatorial Heating, *Clim Dyn, DOI: 10.1007/s00382-018-4169-4*

In section 6.2 we have discussed the basic large-scale circulation adjustment mechanisms to a localized SST anomaly. In this section mechanisms for regional rainfall responses to a localized equatorial sea surface temperature (SST)-induced heating anomaly will be discusses (e.g. ENSO-induced as shown in Fig. 23). It is mainly based on the paper Hamouda and Kucharski (2018) and references therein. This is an important topic as rainfall modifications due to, for example, ENSO can have substantial positive and negative effects and the understanding of the physical mechanisms for such responses is important to assess seasonal predictability. In the literature, several mechanisms have been proposed for rainfall responses to ENSO and other tropical SST-induced heating anomalies (e.g. see Fig. 23). These include:

a) Destabilization in the region with strong SST anomalies, stabilization of the atmosphere in the surrounding regions. This leads to increased convective rainfall in the regions with substantial SST anomalies, and to reduced convective rainfall outside. The stabilization is induced by the upper-level tropical wave propagations (equatorial Rossby and Kelvin waves) discussed in section 5, which spread the signal in the tropical belt.

b) Upper-level convergence in the region surrounding the heating, which compensates for the upper-level divergence in the heating region. This may, according to the continuity equation in pressure coordinates, 44, induce vertical velocities driven from the upper-levels.

c) Flow induced by the heating in remote regions which may be forced to rise because of orography.

d) Ekman pumping induced by remote atmospheric responses (e.g. Gill response discussed in section 6.3) to the heating.

e) Changes of the tropical meridional temperature gradients induced by land masses that drive monsoons. These changes are also communicated from region with the SST perturbation to other tropical regions by equatorial wave propagation.

There are more mechanisms which have been proposed in the scientific literature for rainfall responses to an SST anomaly, but the above list contain the most commonly used hypothesis. Here we will use an idealized *aquaplanet* (explain!)

modelling approach that eliminates the hypothesis c) and e), and leaves the hypothesis a), b) and d). Such an aquaplanet setting has the advantage that some of the complexities in the real world (e.g. land-surface interactions) that make understanding of the responses very difficult, are removed, while the basic dynamical feedbacks are retained. Fig. 37 shows the ICTPAGCM (SPEEDY) models climate in such an aquaplanet setting. All fields shown are annual means.
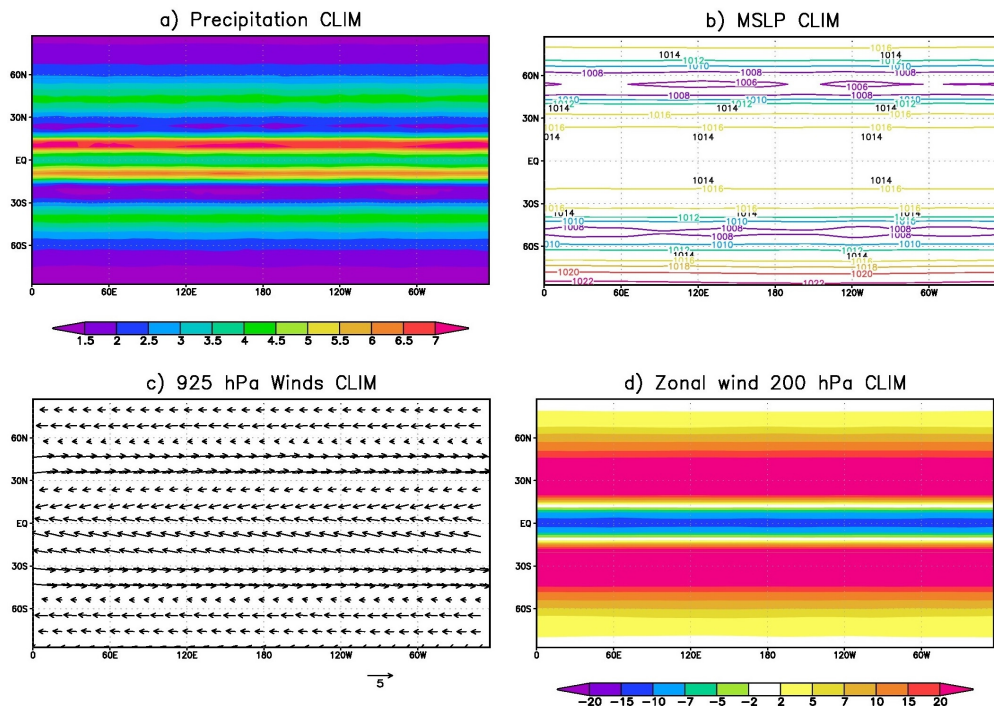

Figure 37: Aquaplanet annual mean climatologies of a) precipitation [mm/day], b) mean sea level pressure [hPa], c) surface winds [m/s] and d) 200 hPa zonal winds [m/s]

Now, the response to a gaussian Gill-type SST anomaly is analysed. For this purpose an additional experiment is performed in which such an anomaly is added to the aquaplanet SST field (Fig. 38). The responses of mean surface pressure, zonal wind, 200 hPa velocity potential, 200 hPa eddy streamfunction, precipitation and 850 hPa pressure vertical velocity are shown in Fig. 39. This response may be interpreted as the Gill-type response reproduced by an Atmospheric General Circulation Model (AGCM). Indeed, in the surface pressure we can identify off-equatorial Rossby-gyres to the west and high pressure at the equator resembling the Kelvin-wave type response. The precipitation and 850 hPa pressure vertical velocity response match each other quite closely, which may not be surprising because on one hand upward motion will lead to condensation (remember lecture course on EST). On the other hand, as discussed in section 6.2, in the tropics there is an

approximate equilibrium between the diabatic heating (cooling) and the adiabatic cooling (warming) term (see equation 173)

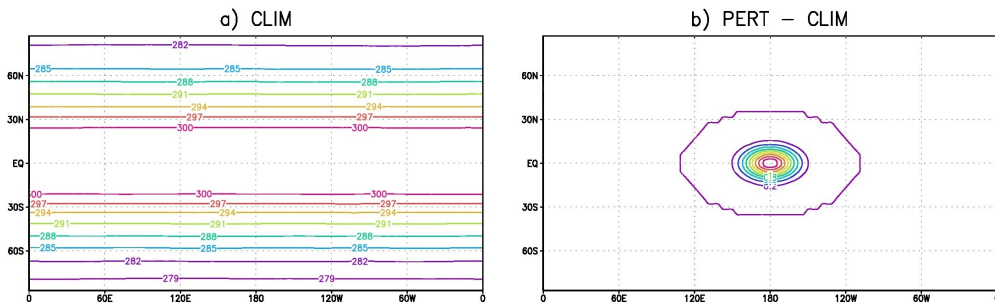$$-S_p \omega \approx \frac{Q}{cp} \quad . \tag{224}$$

Figure 38: Aquaplanet annual mean SST distribition and Gill-type SST perturbation. Units are K.

Also this leads to a good agreement between precipitation (e.g. vertical integrated heating) and the vertical velocity field. Note, however, that in the Gill solution there is no precipitation, and the vertical velocity field is very different from the one shown in Fig. 39 (there we have sinking motion everywhere outside the heating region). These differences are a weakness of the simplified equations used in the Gill solution (essentially modified shallow water equations) rather than a weakness of the AGCM solution, which essentially solves the full Navier-Stokes equations. Another important difference with respect to the traditional Gill solution is that there is an infinite zonal domain is assumed, whereas in reality it is periodic. This leads to differences in the atmospheric adjustments to the heating. For example, to the east of the heating, we do find off-equatorial anticyclonic Rossby gyres in the surface pressure, which resemble the cyclonic ones to the west. We may interpret these as response to the upper-level convergence (maximum in velocity potential) at around 60W to 30W. However, we do note that in the regions with the imposed SST anomaly (around 180E), we get increased rainfall (heating) due to the destabilization of the atmosphere. The rainfall structure appears to be related to the meridional zonal wind gradient (main component of vorticity), which is cyclonic in the off-equatorial regions to the west, and anticyclonic in the off-equatorial regions to the east of the heating (explain!), which should, according to the section 7, induce rising and sinking motion respectively (e.g. from Eq. 221). However, since we are using a numerical model to simulate the effects of Ekman pumping, it is best to use the model's boundary-layer parameterization, which is slightly different. Using the definition
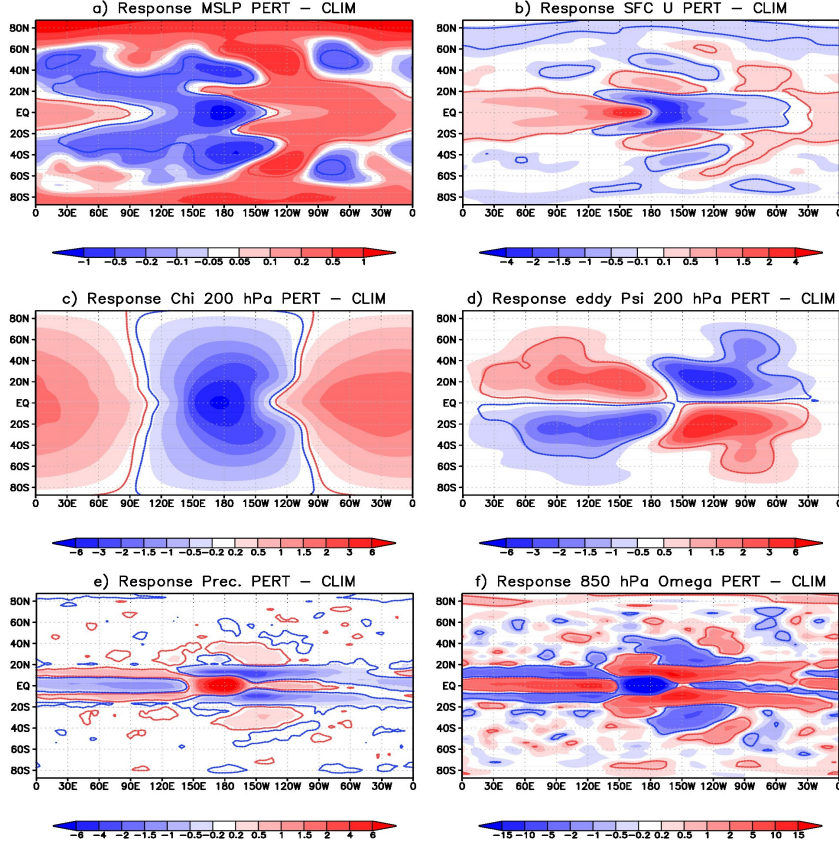
$$|v_0| = \sqrt{u^2 + v^2 + V_{gust}^2} \tag{225}$$

Figure 39: Response to Gill-type SST perturbation of a) mean sea level pressure [hPa], b) surface zonal wind [m/s], c) 200 hPa velocity potential [10^6 m/s^2], d) 200 hPa eddy streamfunction [10^6 m/s^2], e) precipitation [mm/day] and d) omega at 850 hPa [10^{-3} Pa/s].

where u, v are near surface winds (representative for the mean wind in the whole depth of the boundary-layer of the model), $V_{gust} = 5ms^{-1}$ is representing the effect of sub-grid scale gusts, the equations equivalent to Eqs. 207 become for the AGCM:

$$-Cu\sqrt{u^2 + v^2 + V_{gust}^2} + f(v - v_g) = 0 \qquad (226)$$

$$-Cv\sqrt{u^2 + v^2 + V_{gust}^2} - f(u - u_g) = 0 \qquad (227)$$

where $C = \frac{C_D}{h}$, $C_D = 1.8 \times 10^{-3}$ is the drag coefficient over sea, $h = 1000m$ is the depth of the boundary layer, and the geostrophic wind is u_g, v_g. Also, the AGCM is posed in the pressure coordinate system, and since we want to assess solutions including the equator it is convenient to use the geostrophic forcing in terms of

geopotential height gradients using the geostrophic relation:

$$\mathbf{v}_g = f^{-1}\mathbf{k} \times \nabla\Phi \qquad (228)$$

in pressure coordinates. Since Eqs. 226 and 227 are nonlinear, they are solved numerically for the near surface winds, given the geopotential at 850 hPa (by re-introducing the time derivative as in the exercise 3) of section 7). Note that in Eqs. 226 and 227 the near surface winds are non-zero. Once the solutions are found, the divergence of the near surface wind is calculated and the continuity equation in pressure coordinates, 44, is vertically integrated (assuming the near surface winds are constant) to find the vertical velocity, ω_{ek}, induced by Ekman pumping in the model (1000 m corresponds according to the hydrostatic equation approximately to a pressure change of 100 hPa). The resulting Ekman vertical velocity is shown in Fig. 40, and shows very good agreement with the vertical velocity field at 850 hPa shown in Fig. 39 outside the region where the SST perturbation is present. This indicates that Ekman pumping is indeed a very powerful mechanism to induce vertical motion outside the heating region. Also, the upper-level convergence field is calculated for comparison (Fig. 41). There is also some correspondence of this field with 850 hPa vertical velocity and thus rainfall, but it should be noted that the upper-level convergence field and the ω_{ek} field are not independent (e.g. Ekman pumping could induce vertical velocity, this induces convection and thus upper-level divergence). The thermodynamic mechanism a) turns out to be relevant only in the region with SST perturbation and seems to be largely irrelevant outside that region.
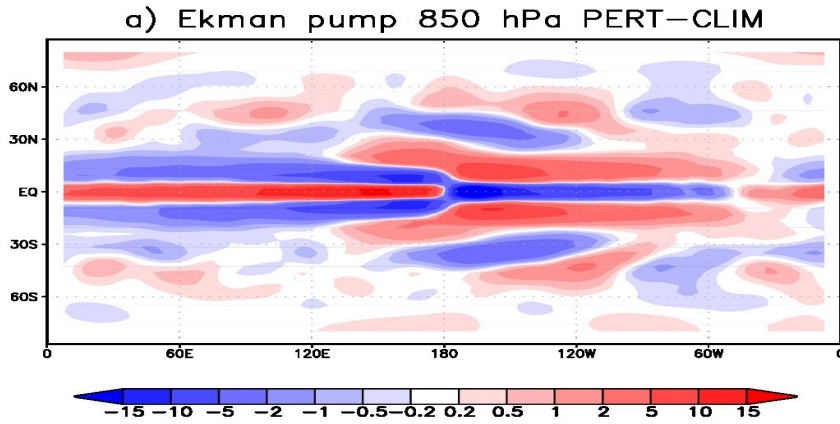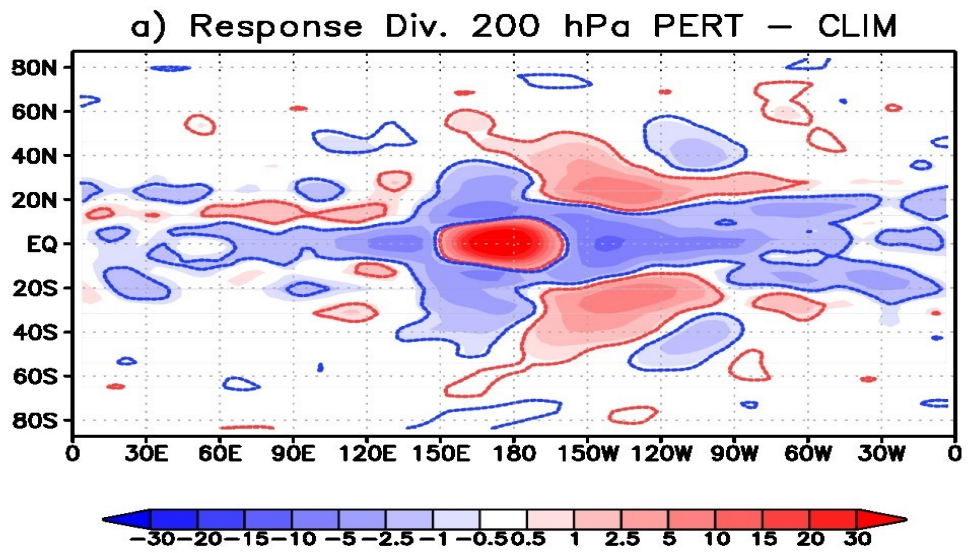

Figure 40: Ekman pumping induced ω_{ek} $[10^{-3}$ Pa/s$]$.

Figure 41: Response in 200 hPa divergence [1/s].